Modeling and analysis of seawater intrusion in the coastal aquifer of eastern Cap-Bon, Tunisia

Claudio Paniconi*, Ihsen Khlaifi†, Giuditta Lecca*, Andrea Giacomelli*, and Jamila Tarhouni†

*Center for Advanced Studies, Research and Development in Sardinia (CRS4)
Cagliari, Italy

†Institut National Agronomique de Tunisie (INAT)
Tunis, Tunisia

email: cxpanico@crs4.it

submitted June, 2000
revised August, 2000

Keywords: Saltwater intrusion, GIS, unsaturated zone, coastal aquifers, numerical modeling, field application

Abstract

A numerical model that treats density-dependent variably saturated flow and miscible salt transport is used to investigate the occurrence of seawater intrusion in the "Korba" aquifer of the eastern coast of Cap-Bon in northern Tunisia. We examine the interplay between pumping regimes and recharge scenarios and its effect on the saline water distribution. More localized simulations are used to examine, in vertical cross sections, the effects of well location and soil type and the role of the vadose zone in possible remediation actions. The exploratory simulations suggest interesting interactions between the unsaturated zone and the saltwater–freshwater interface with possible implications for groundwater exploitation from shallow unconfined coastal aquifers, involving in one case feedback between seawater intrusion and the high pressure head gradients around the pumping-induced drawdown cone and in another case threshold-like interface displacement for tight soils such as clays. The data processing steps undertaken in this GIS and modeling study are described in some detail, and a critical assessment is given of the data availability and of the requirements for successful monitoring and modeling of seawater intrusion risks in heavily exploited coastal aquifers such as those found in the semi-arid regions of the Mediterranean basin. It is shown how, with the aid of GIS, reasonably reliable information can be assembled from maps, surveys, and other sources of geospatial and hydrogeological data, an approach that is necessary in the many regions of the world with acute water resource problems but with limited means for undertaking systematic data acquisition and environmental monitoring actions. Nonetheless the need for more concerted monitoring of relevant parameters and processes and of closer coordination between monitoring and modeling is stressed. An idea of the extent of over-exploitation of the Korba aquifer is obtained by examining the pumping and rainfall/infiltration data, and the simulation results support groundwater pumping as the mechanism for and seawater intrusion as the origin of the salt contamination observed in the soils and subsurface waters of the Korba plain.

1 Introduction

Groundwater is a precious resource in the arid to semi-arid coastal areas of southern Europe, northern Africa, and the Middle East, and is increasingly subject to over-exploitation for agricultural, urban, and industrial uses. In the delicate equilibrium between subsurface seawater and freshwater regimes in coastal areas, prolonged overpumping of groundwater can lead to inland encroachment and/or vertical upconing of the interface (transition or mixing zone) between these regimes, causing salt contamination of freshwater aquifers and salinization of soils [*Sherif and Singh* 1996; *Bear et al.* 1999]. Contamination by salt deteriorates water quality; a two to three percent mixing with seawater makes freshwater unsuitable for human consumption, and slightly higher levels make it unusable for agriculture and irrigation.

A proper assessment of the environmental impacts and economic consequences associated with seawater intrusion phenomena requires monitoring and analysis of the short, medium, and long-term response of the threatened system. It is important to adequately characterize the aquifer flow regime and its natural patterns of land recharge and sea discharge. For heavily-utilized aquifers in semi-arid regions, the flow regime will be particularly sensitive to replenishment by irrigation, artificial recharge, and the rainfall that effectively infiltrates and is not directly lost to surface runoff and evaporation. Such analysis and characterization of the dynamics of coastal aquifers, as with general hydrological systems, can be effectively carried out with appropriate tools such as geographic information systems (GIS), visualization and image processing software, and simulation models [*Paniconi et al.* 1999]. This paper reports on the first results of a modeling study undertaken for the Korba aquifer of northeastern Tunisia, focusing in particular on the role of the unsaturated zone in the various mechanisms for surface recharge and in its interactions with the underlying aquifer and the saltwater–freshwater interface. This work is part of a larger international study aimed at the establishment of a data organization and modeling framework for three important Mediterranean and Atlantic coastal aquifers in Italy, Tunisia, and Morocco [*Paniconi* 1999].

Salt is nonreactive, and thus as a solute it is not as complex to model as other substances which undergo chemical and biological transformations in soils and aquifers. On the other hand, the presence of salt alters water density in such a way as to induce important effects on the pressure and flow fields and thereby on the dynamics of the system [*Kolditz et al.* 1998], and these effects can pose their own mathematical and numerical difficulties. Proper simulation of so-called density-dependent phenomena in groundwater flow and transport relies on coupled models that incorporate the constitutive relationship between solute concentration and density. In the case of seawater intrusion, vertical flows are also important, given the relevance of groundwater pumping in causing the phenomenon, the influence of surface recharge mechanisms, and the role of gravitational forces in driving denser saltwater downwards.

Early modeling studies replaced the disperse transition zone representing the saltwater–freshwater interface with a sharp front and introduced other simplifications such as quasi-three-dimensional layered aquifers or the the Dupuit assumption of predominantly horizontal flow [*Schmorak and Mercado* 1969; *Collins and Gelhar* 1971; *Strack* 1976; *Mercer et al.* 1980; *Wirojanagud and Charbeneau* 1985; *Essaid* 1990]. More recent two and three-dimensional models have introduced coupling, dispersion, and vertical flow (e.g., *Voss and Souza* [*1987*], *Galeati et al.* [*1992*], and *Ségol* [*1993*]). Few existing models, however, consider the unsaturated zone, important for treating ground sources of saltwater such as contaminated irrigation water, for studying soil salinization processes, and, in this study, for illustrating the influences of artificial recharge and natural infiltration as dictated by soil type and other factors.

2 The Korba study site

The 438 km^2 Korba coastal aquifer is situated in the northeastern Cap-Bon peninsula of Tunisia (Figure 1). It is an important touristic, industrial, and, above all, agricultural area, with a population approaching 100 000 concentrated along the coast around the towns of Kelibia in the north and Korba and Ras Marmoura in the south. The coastal plain is bounded by the Mediterranean Sea in the east and by the Djbel Sidi AbedErrahmen mountains (anticline) in the west. The climate is semi-arid, and mean annual precipitation is 460 mm with high annual and inter-annual variability. The wettest months are November–March, and the driest July and August. Effective infiltration (rainfall minus evaporation and surface runoff) is estimated to be less than 10% of annual precipitation and as low as 5–7%. Another possible source of natural recharge for the Korba aquifer is flow across the western mountain range, and, as with evaporation and runoff, reliable data on this variable are not readily available. The study area comprises three ephemeral rivers (*owed*) that are completely dry in the summer, and associated lower order streams. This channel network, when not dry, is fed by rainfall and by runoff from the Djbel Sidi AbedErrahmen mountains.

Increasing population and agricultural activities through the past four decades have led to a steady increase in the amount of water that is pumped from the Korba aquifer; there are currently over 7000 wells that supply the many small farms and communities in the region. Saltwater contamination was first observed in the early 1970s and was recognized as a serious problem in the mid-1980s. A monitoring network of 99 wells was set up in 1996 for acquisition of field data every six months, and this data, along with measurements collected from abandoned agricultural wells in 1962 and 1977, show a marked trend towards decreasing water table levels and increasing concentrations of salt in the unconfined aquifer, with peak salinity values of 5–8 g/l. (Figures 2 and 3). Of note in the latest of the three datasets plotted in Figure 2 are the localized drops in water table to below sea level and the concentric drawdown patterns that have formed. The deterioration in water quality over the observation period is clearly evident from Figure 3, and the concentric patterns that are apparent in the latest dataset here as well suggest a strong and direct link between groundwater exploitation and saltwater intrusion. The fact that the densest clusters of pumping wells are located along the coast makes it plausible that the source of saltwater is the adjoining sea and underlying seawater-saturated formations and that upconing and inland migration of the saltwater–freshwater interface are important mechanisms determining the salinization of the Korba region.

The socio-economic consequences of piezometric drawdown, saltwater intrusion, and salinization in the Korba coastal plain include degradation of arable soils and abandonment of farms, a deterioration in the quality of water pumped from wells and used for irrigation, a decrease in aquifer yields from existing wells, and a migration of the local population in search of alternative freshwater sources [*Khlaifi* 1998]. Several remediation options are being studied for the region, including rationalization and regulation of well pumping, artificial recharge of the aquifer (some pilot trials using treated wastewater have been conducted in a small area in the southern part of the aquifer), and construction of small reservoirs to serve as an alternative source of irrigation water, all within an overall view towards improved management and planning not only of the aquifer but also of land use practices, which clearly have significant impact on the subsurface water regime. Modeling and data analysis will play a key role in the assessment of remediation alternatives and the definition of an appropriate management framework. This contribution is limited to more specific aims related to data organization with a critical assessment of the existing dataset, to model implementation with suggestions for alternative discretizations and additional scenarios that can be investigated, and to exploratory simulations focused on pumping and recharge interactions via the unsaturated zone.

3 Data processing

Aside from the three observation-well measurement campaigns described previously and rainfall records collected from five gauges, data acquisition aimed at monitoring the quality and use of the Korba aquifer has been sporadic until 1996, and no field studies aimed specifically at implementation and calibration of a groundwater transport model have been conducted. This is a common situation for the countries of the Mediterranean basin, and presumably in many other regions worldwide, where environmental protection is not a high priority and lack of funding has prevented systematic and coordinated monitoring efforts. Nonetheless, for the Korba site a large amount of data has been accumulated since the early 1960s from a variety of sources and surveys, and for this study a large effort was expended on the organization and manipulation of these data, and on deriving and inferring from them parameters and boundary conditions for the model discretization and implementation.

The available data for the Korba site include topographic and soil maps, geological and geophysical surveys, water level and water quality measurements taken from the monitoring wells, information relating to agricultural activities and water use, hydrographic and geomorphologic characterizations, and data from meteorological stations. A geographic information system was used to organize these diverse data and to support both pre- and post-processing tasks connected with the saltwater intrusion modeling [*Giacomelli et al.* 1999]. Some of the processing, support, and analysis functions performed with the GIS include:

- Basic digitizing and manipulation to create data layers and thematic maps: all geographic data was initially available in paper format and at different scales and classifications, and required georeferencing, mosaicking, and assigning of attribute information;
- Data conversion and formatting to adapt GIS-processed data for input to the simulation model and to enable GIS-based 2D visualization and comparison of model output. Scientific visualization software was used for 3D and 4D (space and time) analysis of simulation results, but also in this case GIS-based routines were used for data conversion and formatting;
- Multicriteria analysis for recharge optimization: a simple analysis was conducted to identify areas in the Korba region that might be most suitable for artificial recharge of the aquifer, based on a weighted combination of soil, aquifer transmissivity, geology, and terrain slope map features. This was a preliminary and heuristic analysis but illustrates a potentially important application for combining observation data and simulation results through GIS to produce qualitative or quantitative indices useful for remediation studies and more general water resources management.

The data most relevant to the modeling study and that required the most intensive GIS processing were the geological and terrain maps and the historical data from the monitoring and pumping wells and rain gauges, as described below.

For modeling purposes, it was necessary to process extremely detailed geological data and to identify and aggregate the features pertinent to the coastal aquifer. The resulting map is shown in Figure 4. The unconfined aquifer, formed during the Pliocene and Quaternary ages by deposition of eroded products from the Djbel Sidi AbedErrahmen anticline and the Dakhla syncline, is underlain by a Miocene marl formation and below this stratum by a small and less-exploited confined aquifer. The Pliocene formation is a sandstone with alternating marl units, while the Quaternary alluvium is composed of detrital sediment (sand, gravel, and silt) with thin clay lenses. The sandstone formation spans the entire aquifer and has a mean thickness of 85 m, while the detrital formation is less ubiquitous and has a thickness that varies between 20 and 25 m. In some parts of the Korba region the two formations overlap, as can be seen in Figure 4. In the model these dominant Pliocene and Quaternary formations are treated as a single unconfined aquifer, albeit assigning to each formation different values for the main hydrogeological parameters; in essence treating the aquifer as a single unit with block heterogeneity. An additional characteristic geomorphologic feature of the Korba plain is the dune formation that runs along part of the coastline just east of the second, smaller Menzel Temime anticline. This unit is composed of Quaternary sediments with high hydraulic conductivity, but was not modeled as a distinct block given its small vertical and lateral dimensions relative to the other two formations. The dunes were only indirectly considered in a set of artificial recharge simulations reported below. Less dominant features such as the marl units and clay lenses were also ignored, owing to lack of data and the need to simplify the model representation of the study area. In the same manner it was impossible to determine the precise extent, laterally and vertically, of the main formations, and the parameter values assigned to the these two blocks or were inferred from a combination of observation data and information from previous Korba studies, published values for comparable geological units, and, for the conductivity values, some calibration. The main intent was to capture the dominant features, and to illustrate that complex configurations can be easily supported by the GIS and model, given adequate data. This applies also to the terrain and historical data.

Topographic maps were used to interpolate a 50x50 m digital elevation model (DEM) for the study area, and, in conjunction with geological data, to define the surface limits of the aquifer and its base configuration (Figure 5). The topography ranges from 0 to 161 m a.s.l., and the aquifer thickness is also highly variable, with a mean of about 85 m corresponding to the thicker and more extensive sandstone formation, a range from 151 m in the south to 24 m in the north, and a decreasing trend from east to west to nearly vanish at the Djbel Sidi AbedErrahmen mountains. With the geometry and dimensions of the aquifer thus delimited, a triangulated irregular network (TIN) was constructed with the GIS and then used to generate the 2D surface grid for the model. The advantage of using GIS rather than standard unstructured grid generation software is that the GIS enabled a direct link to be maintained between the mesh structure and the geographic data on which it is based. For instance, distance from the coast, location and importance of pumping wells, and location of monitoring wells were all considered in determining the local grid resolution, and in the future other considerations (designated artificial recharge areas, characteristics of surface freshwater reservoirs and other water bodies) can also be easily incorporated. The disadvantage is that a GIS will not have optimization features as sophisticated as those found in specialized grid software that automatically generate a mesh with geometrical properties that ensure numerical stability, accuracy, or convergence of the model, so in practice some degree of trial-and-error is used to obtain an adequate mesh.

Imposition of surface boundary conditions was also assisted by the GIS, incorporating information from the pumping and monitoring well datasets, derived irrigation maps, and rainfall records into the nodes or triangles of the 2D grid. A further advantage of the TIN-based grid is that its elements can be converted to geographic data coverages in either point format, representing computational nodes, or polygon format, representing the mesh triangles. The more than 7000 pumping wells present in the Korba region were clustered into a more manageable handful of model sink nodes, with penetration depths of approximately 25 m where the aquifer is shallow and approximately 45 m where it is thicker. To the best available knowledge, the total volume of water pumped from the aquifer in recent years is close to 50×10^6 m^3/yr. Pumping volumes, together with irrigation rates, are difficult to estimate reliably for the Korba site, given also the abundance of small-farm private wells in the region. In the absence of data for earlier years, the simulations were run under various scenarios, for example using a linearly increasing yearly pumping rate over a 35-year simulation period, from 0 for 1962 to some fraction (given that the pumping was concentrated at a few well clusters) of the estimated 50×10^6 m^3 for 1996. Irrigation rates estimated from available maps were lumped into the effective infiltration term. Annual rainfall data is more reliable, but the problem in this case is lack of detailed information on rainfall rates at small temporal scales (hourly and even finer resolution). This is critical if the unsaturated zone component of the model is to accurately simulate rainfall–runoff–infiltration partitioning and thereby reproduce an important natural recharge component of the aquifer's water balance. In absence of this detailed data, scenario simulations were again run, and, in particular, the estimated effective infiltration of (less than) 10% of annual rainfall was relied on. It is interesting to note that, based on these estimates and using 40 mm as effective annual infiltration, the volume of water recharged to the aquifer from a combination of rainfall and irrigation is approximately 18×10^6 m^3 annually; comparing this value with the 50×10^6 m^3 estimated current annual pumping rate gives an idea of the degree of over-exploitation of the aquifer.

4 The CODESA-3D model

The numerical model used in the study is a distributed, fully three-dimensional saturated–unsaturated finite element code that makes no assumptions regarding the nature of the saltwater–freshwater interface or the flow regime in the aquifer and can account for spatial and temporal variability in parameters and boundary conditions. The wide applicability of the model allows investigation of a number of scenarios important for the Korba study site, such as the effects of: aquifer geometry, heterogeneity, and dispersivity; location and rate of pumping, recharge, and irrigation; rainfall–runoff–infiltration partitioning; soil and unsaturated zone characteristics; and coastal boundary conditions including treatment of the freshwater outlet "window". The full coupling in the model between the water flow and salt transport components makes it possible to examine in detail density effects and the interactions between the pressure head and salt concentration fields, and, derived from these fields, the pressure gradients, water table levels, groundwater velocities, and saltwater–freshwater interface.

The numerical model, CODESA-3D (COupled variable DEnsity and SAturation), is described in detail in *Gambolati et al.* [*1999*] and its mathematical aspects are briefly reviewed here for purposes of introducing some basic concepts and the important parameters involved in the simulations to be subsequently presented. Numerically, the model uses a standard finite element Galerkin scheme, with tetrahedral elements and linear basis functions, complemented by weighted finite differences for the discretization of the time derivatives [*Zienkiewicz* 1986] (in the runs reported here Crank-Nicolson weighting was used for both the flow and transport equations, with no mass lumping). Sophisticated algorithms are used to handle the coupling and nonlinearity inherent in the seawater intrusion model and for solving the large sparse systems resulting from discretization and linearization of the model equations. In addition, for computational efficiency dynamic time stepping is implemented to ensure that the code uses large time steps where possible, based on whether the convergence of the iterative coupled solution at a given time is fast (time step is increased), intermediate (time step is unaltered), or slow (time step is reduced). For the 35-year simulations to be described, this adaptive temporal discretization resulted in time steps as small as 3 hours (10^4 seconds) and as large as 3 years (10^8 seconds).

The mathematical model of density-dependent flow and transport is expressed in terms of an equivalent freshwater total head h, defined as [*Frind* 1982; *Huyakorn et al.* 1987]

$$h = \psi + z \tag{1}$$

where $\psi = p/(\rho_o g)$ is the equivalent freshwater pressure head, p is the pressure, ρ_o is the freshwater density, g is the gravitational constant, and z is the vertical coordinate directed upward. The density ρ of the saltwater solution is written in terms of the reference density ρ_o and the normalized salt concentration c:

$$\rho = \rho_o(1 + \epsilon c) \tag{2}$$

where $\epsilon = (\rho_s - \rho_o)/\rho_o$ is the density ratio and ρ_s is the solution density at the maximum normalized concentration $c = 1$ (e.g., the density of seawater). The dynamic viscosity μ of the saltwater mixture is also expressed as a function of c and of the reference viscosity μ_o as

$$\mu = \mu_o(1 + \epsilon' c) \tag{3}$$

where $\epsilon' = (\mu_s - \mu_o)/\mu_o$ is the viscosity ratio, μ_o is the freshwater viscosity, and μ_s is the viscosity of the solution at $c = 1$. Viscosity effects are often ignored in seawater intrusion modeling studies ($\epsilon' = 0$ is assumed), although further study of this term is warranted. Density effects, on the other hand, are non-negligible and important, with typical values of ϵ for oceans and open seas being 0.025–0.030.

With these definitions, the coupled system of variably saturated flow and miscible salt transport equations is

$$\sigma\frac{\partial\psi}{\partial t} = \nabla\cdot\left[K_s\frac{1+\epsilon c}{1+\epsilon' c}K_r\left(\nabla\psi + (1+\epsilon c)\eta_z\right)\right] - \phi S_w \epsilon\frac{\partial c}{\partial t} + \frac{\rho}{\rho_o}q \tag{4}$$

$$\mathbf{v} = -K_s\frac{1+\epsilon c}{1+\epsilon' c}K_r\ \left(\nabla\psi + (1+\epsilon c)\eta_z\right) \tag{5}$$

$$\phi\frac{\partial S_w c}{\partial t} = \nabla\cdot(D\nabla c) - \nabla\cdot(c\mathbf{v}) + qc^* + f \tag{6}$$

where σ is the general storage term or overall storage coefficient, t is time, ∇ is the gradient operator, K_s is the saturated hydraulic conductivity tensor, K_r is the relative hydraulic conductivity, η_z is a vector equal to zero in its x and y components and 1 in its z component, ϕ is the porosity, $S_w = \theta/\theta_s$ with θ the volumetric soil moisture content and θ_s the saturated moisture content (generally equal to porosity), q is the injected (positive)/extracted (negative) volumetric flow rate, $\mathbf{v}$ is the Darcy velocity vector, D is the dispersion tensor, c^* is the solute concentration in the injected/extracted fluid, and f is the volumetric rate of injected/extracted solute that does not affect the velocity field.

σ, K_r, and D are nonlinear coefficients which depend on the solution, and need to be elaborated further. The pressure head dependencies in the relative hydraulic conductivity and general storage terms for the case of variably saturated flow are commonly expressed through semi-empirical characteristic relations such as those of *Brooks and Corey* [*1964*]

$$\begin{aligned} S_e(\psi) &= (\psi_s/\psi)^{\beta_b} & \psi < \psi_s \\ S_e(\psi) &= 1 & \psi \geq \psi_s \end{aligned} \tag{7}$$

$$\begin{aligned} K_r(\psi) &= (\psi_s/\psi)^{2+3\beta_b} & \psi < \psi_s \\ K_r(\psi) &= 1 & \psi \geq \psi_s \end{aligned} \tag{8}$$

or of *van Genuchten and Nielsen* [*1985*]

$$\begin{aligned} S_e(\psi) &= (1+\beta_v)^{-\gamma} & \psi < 0 \\ S_e(\psi) &= 1 & \psi \geq 0 \end{aligned} \tag{9}$$

$$\begin{aligned} K_r(\psi) &= (1+\beta_v)^{-5\gamma/2}\left[(1+\beta_v)^{\gamma} - \beta_v^{\gamma}\right]^2 & \psi < 0 \\ K_r(\psi) &= 1 & \psi \geq 0 \end{aligned} \tag{10}$$

where S_e is the effective saturation defined as $(\theta - \theta_r)/(\theta_s - \theta_r)$, θ_r is the residual moisture content, β_b is a fitting constant, ψ_s is the capillary or air entry pressure head value, $\beta_v = (\psi/\psi_s)^n$, n is a fitting constant, and $\gamma = 1 - 1/n$ for n approximately in the range $1.25 < n < 6$. The corresponding general storage term is

$$\sigma = S_w S_s(1+\epsilon c) + \phi(1+\epsilon c)\frac{dS_w}{d\psi} \tag{11}$$

where S_s is the specific storage of the aquifer. Expressed in this way the general storage term is applicable to both aquifers ($S_w S_s$ term in (11), with $S_w = 1$) and unsaturated soils ($dS_w/d\psi$ term dominant). Figure 6 shows typical saturation–pressure head and conductivity–pressure head curves for three representative classes of soils, clay, silt-loam, and sand-loam, as computed from the Brooks-Corey functions.

The dispersion tensor $D = \phi S_w \tilde{D}$, where $\tilde{D}$ is defined as in *Bear* [*1979*], is given by

$$D_{ij} = \phi S_w \tilde{D}_{ij} = \alpha_T \mid \mathbf{v} \mid \delta_{ij} + (\alpha_L - \alpha_T)\frac{v_i v_j}{\mid \mathbf{v} \mid} + \phi S_w D_o \tau \delta_{ij} \qquad i,j = x,y,z \tag{12}$$

where α_L and α_T are the longitudinal and transverse dispersivity coefficients, respectively, $\mid \mathbf{v} \mid = \sqrt{v_x^2 + v_y^2 + v_z^2}$, δ_{ij} is the Kronecker delta, D_o is the molecular diffusion coefficient, and τ is the tortuosity ($\tau = 1$ is usually assumed). The accuracy of finite element numerical solutions of the transport equation (6) is strongly conditioned on the relative strengths of the dispersion term $\nabla\cdot(D\nabla c)$ and the advection term $\nabla\cdot(c\mathbf{v})$, as advection-dominated transport is characterized by sharp concentration fronts which are difficult to resolve (spurious oscillations are generated) unless a sufficiently small mesh is used. For realistic three-dimensional problems excessively small grids cannot be used due to computer CPU and memory constraints, and so the dispersivity coefficients are often assigned artificially high values. Alternatives to finite element methods, such as upwind finite volume techniques, show promise in overcoming the numerical difficulties associated with advection-dominated transport [*Putti et al.* 1990].

Coupling in system (4)–(6) is due to the concentration terms in the flow equation (4) and the head terms that appear in the transport equation (6) via the Darcy velocities. The system is mathematically irreducible and any sequential solution procedure requires iteration. The nonlinearity of the coupled system is due to the dependence of solution density and viscosity on concentration that arises from relationships (2) and (3). The saturated flow equation is not as strongly nonlinear as the transport equation, and the importance of coupling and the degree of nonlinearity in the transport equation is expected to decrease as ϵ decreases or as dispersion becomes dominant [*Putti and Paniconi* 1995]. An additional source of nonlinearity is introduced when the unsaturated zone is included in the saltwater intrusion model, as expressed through equation (4) and its conductivity and storage coefficients. These are strong nonlinearities which can introduce difficulties in the numerical solution of the flow problem [*Paniconi and Putti* 1994].

5 Model discretization, parameters, and boundary conditions

The first step in the discretization of the study domain for model simulation was the generation of the DEM-derived TIN-based 2D surface grid described earlier, resulting in a mesh containing 2917 triangles and 1643 nodes (Figure 7). This unstructured grid, constructed so as to have the smallest elements (28.6 m^2 as compared to 1.48 km^2 for the largest) along the coast and around zones of heavy groundwater pumping, was then replicated vertically for 6 layers, yielding a 3D mesh of 52506 tetrahedral elements and 11501 nodes. The layers were defined to be of increasing thickness from the surface to the base of the aquifer (proportionally 6, 12, 18, 18, 23, and 23%) so as to have a sufficiently fine resolution for investigating unsaturated zone processes. With this configuration of just over 10000 nodes, a typical 35-year transient simulation on a mid-range workstation required about 1 hour of CPU, a fast enough turnaround time for these first phases of the study where frequent runs were needed for fine-tuning the model and for generating scenarios. A much finer resolution (more than 100 000 nodes) will be needed in future simulations to examine in more detail the three-dimensional behavior of selected processes and to relax the dispersivity constraints (the values used in the simulations reported here were $\alpha_L = 170$ m and $\alpha_T = 17$ m; values for the other solute transport parameters were 0.030 for the density ratio ϵ, and 0 for both the viscosity ratio ϵ' and the molecular diffusion coefficient D_o).

The CODESA-3D model can in theory assign different flow and transport parameters to each vertical layer and each tetrahedral element; for the Korba simulations only selected hydrogeological parameters were treated as spatially variable, in a block heterogeneity sense according to the presence of either Pliocene or Quaternary formations. For the more dominant Pliocene sandstone the x, y, and z components of the saturated hydraulic conductivity tensor K_s were assigned values of $K_x = K_y = 3.4 \times 10^{-6}$ m/s and $K_z = 9.0 \times 10^{-6}$ m/s, and the porosity ϕ (or θ_s) was set at 0.27. For the sparser and thinner Quaternary alluvium the corresponding parameter values were $K_x = 3.4 \times 10^{-5}$ and 1.4×10^{-7} m/s for the top 2 layers respectively, $K_y = 3.4 \times 10^{-5}$ and 3.4×10^{-7} m/s for the top 2 layers, and $K_z = 9.0 \times 10^{-5}$ m/s and $\phi = 0.30$ for both layers. Aquifer specific storage $S_s = 1.0 \times 10^{-5}$ m^{-1} and Brooks-Corey parameters $\beta_b = 3.3$, $\psi_s = -0.25$ m, and $\theta_r = 0.02$ were used for both formations. The above values correspond to the "sand-loam" soil/aquifer considered for most of the simulations described in the following section (see Figure 6). For the "clay" simulation of the third scenario saturated hydraulic conductivities one order of magnitude smaller were used, along with $\phi = 0.45$ for the Pliocene formation and 0.48 for the Quaternary, and Brooks-Corey values $\beta_b = 0.44$, $\psi_s = -0.9$ m, and $\theta_r = 0.02$.

The irregular geometry of the aquifer, in particular its nonuniform base and thickness arising from the syncline and dune formations, were considered important features in determining the response of the Korba coastal plain to groundwater exploitation and the dynamics of saltwater intrusion, and these features were thus discretized to conform as closely as possible to the available data. It would be interesting to quantify more precisely the effects and importance of variable aquifer thickness, comparing the current discretization with a series of hypothetical configurations including more uniform geometries as usually assumed in reported seawater intrusion studies. For the Korba site such sensitivity analyses could be useful for planning future hydrogeological field studies aimed at augmenting the quantity and accuracy of available data, and for providing additional information to be used in multicriteria assessments of remediation options.

The most important boundaries of the three-dimensional discretized representation of the Korba study site are the land surface (sources and sinks of fresh and/or salt-contaminated water from rainfall, evaporation, irrigation, pumping, artificial recharge, and streams and other surface water bodies), the eastern coastline (discharge of freshwater from the aquifer and source of saltwater from the sea or underlying seawater-saturated porous media), and the western edge of the Korba plain (natural subsurface recharge of the aquifer from adjoining formations). These three boundaries are critical both in the physical role they play in the dynamics between freshwater and saltwater in the aquifer and in the numerical effect they can have in determining simulation outcomes. Imposing constraints on these boundaries which accurately mimic natural conditions is difficult due to (again) lack of information and to the complexity of the boundaries, and there is ample scope here for experimentation and sensitivity analysis. The land surface, for instance, comprises a number of sources and sinks, each of them highly variable in space and time; the western edge may contain significant localized water transmission pathways such as fractures; the coastal boundary should require some prior knowledge of the position of the saltwater–freshwater interface and the extent of the freshwater outlet window. This window portion of the coastal edge is treated as a zero dispersive flux boundary for the solute, allowing lighter freshwater to discharge to the sea, while the nodes below it are assigned a fixed relative concentration value of 1, implying a continous source of heavier seawater that enters the aquifer at depth. The extent or thickness of the window is likely to vary over time, contracting or expanding depending on the hydrological balance of the aquifer system. To capture this variation requires iterative treatment of the coastal boundary condition in the solute transport model, in a manner similar to seepage face handling in models of variably saturated groundwater flow. This is a feature still to be implemented in the CODESA code, so in the simulations reported below the window thickness was kept fixed.

Synthesizing, for the vertical face corresponding to the coastline the boundary conditions for the transport equation were zero dispersive flux for the nodes of the window (the 4 nodes of the topmost 3 layers were designated as window nodes, for a thickness of approximately 30 m) and maximum concentration for the nodes below the window, while vertical hydrostatic equilibrium (fixed actual, not equivalent, total head) was prescribed on all nodes for the flow equation. For the land surface, zero dispersive flux was assigned to all nodes for the transport equation, while for the flow equation the ephemeral streams were ignored and the estimated irrigation values were incorporated into the effective infiltration rates; these latter values, along with pumping and artificial recharge values used in the various simulations, are described in more detail in the next section. The western edge of the Korba plain was treated in a default manner as a zero flux boundary for both flow and transport, thereby ignoring this potential source of natural subsurface recharge. The remaining boundaries (the northern and southern edges and the bottom of the aquifer) were considered impermeable to both water and salt (zero Darcy and dispersive fluxes). This treatment of the bottom boundary neglects possible water flow (leakage) between the unconfined aquifer and the underlying confined aquifer across the Miocene marl formation, a contribution whose significance needs to be assessed via field investigations.

6 Simulation results

Model simulations of the Korba coastal aquifer that have been performed include preliminary sensitivity and calibration experiments and three scenarios to investigate the interplay between pumping regimes, effective infiltration, and artificial recharge. The preliminary simulations, reported in *Khlaifi* [*1998*] and *Lecca et al.* [*1998*], were used to fine tune the model and establish starting conditions for the scenario runs. Different boundary configurations, grid discretizations, and parameter combinations were tried, and it was observed that the model response was particularly sensitive to effective infiltration rates and saturated conductivities. In calibration trials based on steady state flow simulations, these parameters were varied, within the bounds of available field measurements, until an adequate match was obtained with the observed 1962 piezometric data. The resulting pressure head distribution and water table levels (Figure 8) were then used as the initial flow conditions for subsequent transient simulations using the fully coupled model (for the transport component in these transient simulations, a zero concentration initial condition was used throughout the domain so as to simulate migration of a saltwater front from the sea boundary).

In the three scenarios the "equilibrium state" presumed to exist prior to the 1960s (with little or no groundwater pumping) is subjected to disturbances in the form of regional and localized groundwater exploitation over a 35-year period (1962–96).

The first scenario involves regional groundwater pumping from 10 well clusters extracting a linearly increasing amount of water, from 0 in 1962 to 7.2×10^6 m^3 in 1996. The overall pumping rate is distributed uniformly over the 10 wells, which have a penetration depth of approximately 25 m where the aquifer is shallow and 45 m where it is thicker, as described earlier (in the numerical implementation, the well screen or sink node is situated at the bottom of the third layer from the surface). In the second run of this scenario, local artificial recharge is introduced after 25 years of pumping, with continued extraction over the following 10 years as in the first run. The 10 years of recharge is applied at a source node situated near one of the coastal well clusters, at the same depth and at a constant rate of 3×10^6 m^3/yr. The results of these two runs are shown in Figure 9 for the central portion of the modeled domain. As is to be expected the effect of the recharge is only local, but it is nonetheless successful in reducing both drawdown and salinity in the central coastal portion of the aquifer that was most heavily affected by seawater encroachment in the first run. Coastal recharge of this sort can counteract the sharp "reverse flow" gradients that can form when the localized unsaturated zone and reduced pressure heads that result from groundwater drawdown too near the coast give way to heavy influxes of seawater. In addition, for the Korba study site remediation of heavily salt-contaminated coastal zones by local artificial recharge can exploit the favorable permeabilities associated with the dune formations.

In the second and third scenarios more localized simulations are used to examine, in vertical cross section, the behavior in time of the water table and the saltwater–freshwater interface as groundwater is pumped at different points and under different soil or infiltration conditions. In both scenarios a single well acts as a sink node drawing water from the aquifer at a rate that increases linearly over the 35-year simulation period from 0 to 0.91×10^6 m^3/yr. The results are plotted at times 1, 6, 25, and 35 years for a vertical cross section of length approximately 5 km perpendicular to (and including) the coast and passing through the town of Korba.

In the second scenario inland (about 3.6 km from the coast) and coastal (1.4 km) pumping regimes are compared (Figure 10). A new equilibrium state in terms of the saltwater–freshwater balance is quickly established in the case of inland pumping, with the 0.5 isoline remaining stationary at about 150 m from the coast. On the other hand in the area around the pumping well it is apparent that the extraction rate exceeds the rate of natural recharge (an effective infiltration rate of 22 mm/yr was used) as seen by the severe and non-steady drop in water table. In the case of coastal pumping, under the same conditions of pumping and natural recharge, the reverse is true — drawdown is significantly less but seawater intrusion is much more pronounced and the interface is nonstationary. These effects feed back into eachother: the influx of seawater is spurred by the nearby high pressure head gradients in the unsaturated zone and around the drawdown cone, and in turn this seawater serves as a ready source of water for the pumping well, limiting the water table drop.

In the third scenario the coastal pumping case of Figure 10, where the material properties were those of a sand-loam soil/aquifer, is compared to a case where saturated hydraulic conductivities, porosity, and the parameters of the unsaturated zone hydraulic functions correspond to a porous medium of higher clay content. The clay soil is also presumed to have a lower infiltration capacity, so the annual rainfall that effectively infiltrates was set at a lower value of 15 mm compared to the 22 mm/yr of the sand-loam case. The more severe groundwater drawdown and the greater net (after 35 years) encroachment of seawater observed in Figure 11 for the clay case is likely a result mainly of the lower rate of natural freshwater recharge from the surface applied to this soil. The threshold-like dynamics displayed in the seawater intrusion for the clay case as opposed to the more or less uniform inland progression through time of the 0.5 salinity isolines observed for the sand-loam case may be accounted for by the interplay in the clay soil between low (compared to sand-loam) saturated conductivities, which impede (sea)water being drawn to the pumping well at early times, and high relative conductivities (see Figure 6), which quickly draw water in once the unsaturated zone is sufficiently extended, by drawdown, into the porous medium.

In Figure 12 more detailed concentration isolines at time 35 years are shown for the clay soil/aquifer simulation of Figure 11. From this plot we can conclude that for this scale of aquifer and for the combination of parameter values and boundary conditions adopted for these scenarios, it is important to model dispersion effects in the dynamics of the saltwater–freshwater interface. Extrapolating from the isolines, the width of the transition zone for this scenario can be estimated to be about 1 km, which is significant for a coastal plain such as Korba that is only 5–10 km wide and heavily dependent on groundwater-intensive agriculture. It is also worth noting that the shape and width of the interface varies with depth, and it would be important to investigate, via much more detailed simulation, the factors which are most important in determining the attributes of the saltwater–freshwater interface. In particular, the steep slope of the bed of the aquifer near the coast may play a strong role in this regard, giving rise to large seaward freshwater pressure head gradients which counter the inflow of heavier seawater at the base of the aquifer, thus producing a relatively "straight" interface rather than the slanted interfaces predicted for aquifers with regular properties and geometries. (It should also be noted that the concentration isolines plotted in the vertical cross sections are not as straight as they seem, owing to the distortion in the graphical presentation of the results, where the x axis spans 5 km while the z axis only around 100 m.)

A feature that emerges clearly in the three scenarios presented, and supported by the limited observation data of Figure 3, is that under uniform effective annual infiltration (be it 15 or 22 or 40 mm) but steadily increasing pumping from the aquifer, the saltwater front moves inexorably inland, for a total distance after 35 years of about 800 m (measured by the position of the 0.5 concentration isoline) for the sand-loam coastal pumping scenario and about 1 km for the clay case. The equilibrium-disrupting potential of inland pumping is on the other hand much less pronounced, although drawdown under both inland and coastal pumping regimes can of course have serious impacts independently of saltwater contamination.

7 Discussion and Conclusions

A geographic information system and a three-dimensional coupled variable density and saturation numerical model have been implemented for the Korba coastal aquifer of northeastern Tunisia, and simulations investigating the interplay between pumping regimes, natural and artificial recharge, soil type, the unsaturated zone, and seawater intrusion have been conducted.

GIS provided an essential platform for data management, enabling the organization and merging of a high volume of data that has been collected in often ad hoc manner from diverse sources over the past 35 years. The resulting GIS dataset for the Korba aquifer, in addition to facilitating pre- and post-processing interaction with the model, represents per se an important outcome of this study, since it made possible a critical assessment of data quality and a valuation of data requirements for a successful model-based analysis of seawater intrusion phenomena. Some of the important shortcomings of the existing dataset are: insufficient monitoring data for piezometric heads and aquifer salinity levels; lack of spatio-temporal detail in rainfall, runoff, evaporation, irrigation, and pumping records; and incomplete characterization of aquifer and soil properties such as conductivity, dispersivity, and leakage.

The 99-well monitoring network set up in 1996, if well-maintained and regularly sampled, is invaluable for constructing an adequate historical record of water table and seawater intrusion dynamics in the region, forming a basis upon which to assess future remediation hypotheses and actions. In a region such as the Cap-Bon with thousands of private wells that pump water from the aquifer for irrigation uses, it is extremely difficult to obtain reliable information regarding extraction rates and volumes, and how these are distributed spatially and over time (both seasonally and interannually). One measure that could alleviate this problem in general (as it is a common situation for many coastal regions of the Mediterranean basin) would be to have more effective coordination between the normally distinct institutional agencies responsible for agriculture on the one hand and water resources management on the other. For a relatively small region such as Korba spatial detail in the hydrologic data is not as important as it is for pumping and irrigation data, so long as the natural water balance data that is available is accurate and of high temporal resolution. For an aquifer study estimates of net recharge (effective infiltration) are sufficient when detailed rainfall, runoff, or evaporation data are not available. The rough and annually-averaged natural recharge values used in this study are therefore only indicative. Nonetheless the extent of over-exploitation of the Korba aquifer suggested by the balance between pumping and rainfall/infiltration data is considered realistic, as is the connection between groundwater pumping and seawater intrusion suggested by the monitoring data and supported by the simulation results.

Adequate characterization of aquifer and soil properties to the degree required by a numerical model such as CODESA-3D is arguably a more difficult (and expensive) task than the acquisition of water balance and monitoring well data, but it should be kept in mind that: (i) this type of characterization normally needs to be done only once rather than repeatedly within or over the years; and (ii) a surprising amount of reasonably reliable information can be assembled (with the aid of GIS) from maps, surveys, and other sources of data produced in a variety of contexts unrelated to the study at hand. This was the approach used (out of necessity) in this work, but for more detailed future analysis it will be important to substantiate this data with field and laboratory observations specifically aimed at a groundwater modeling saltwater intrusion study. In particular, pump and tracer tests, geophysical surveys, and laboratory analyses of core and soil samples will provide more accurate estimates of hydraulic conductivity, dispersivities, soil parameters, and the approximate position of the saltwater–freshwater interface.

The simulations performed for the Korba study give an idea of the usefulness of physically-based, distributed numerical models for corroborating and extrapolating observation data, for studying the basic dynamics and response of coastal aquifer systems, for generating scenarios and predictions, and for assessing environmental impacts and remediation strategies. A broad example of this is how the model demonstrates, under coastal pumping scenarios, an inexorable and significant encroachment of the saltwater–freshwater interface when groundwater exploitation and natural replenishment of the aquifer are not in balance.

The exploratory simulations and analyses reported here examined, in three sets of paired simulations, the piezometric, salinity, and unsaturated zone response to local artificial recharge, inland versus coastal pumping, and variations in hydrogeological properties of the porous medium. Local recharge was shown to be effective in counteracting seawater encroachment and groundwater depletion, although its feasibility in particular situations will depend much on the characteristics of the soil and aquifer (e.g., the dune formations along the Korba coast) and on availability of a source for recharge water (treated wastewater is one possible option for Korba). The scenarios for which the simulation results were examined in vertical cross sections perpendicular to the coast suggest some interesting interactions between the unsaturated zone and the saltwater–freshwater interface, involving in one case feedback between seawater intrusion and the high pressure head gradients around the pumping-induced drawdown cone and in another case threshold-like interface displacement for tight soils such as clays. These interactions warrant more detailed analysis given their possible importance in situations of groundwater exploitation from shallow unconfined coastal aquifers. Other simulation results, not restricted to unconfined aquifers, suggest an important role may be played by the geometry and bed slope of the aquifer in determining the shape and penetration of the saltwater–freshwater interface.

There is scope for much further study based on the model of the Korba aquifer. Briefly, some interesting aspects not examined in this work include: the influence of the position of the freshwater outlet window and its interaction with the unsaturated zone; alternative discretizations, in particular a finer mesh, to assess dispersivity effects on the transition zone and to incorporate the coastal dune formations as a distinct hydrogeologic unit; more elaborate pumping and artificial recharge scenarios, coupled with GIS analysis that combines semi-quantitative terrain, soil, and aquifer features, to identify appropriate zones for freshwater injection; simulation of the benefits of improved soil management such as terraced soils and small water-capture basins that allow for enhanced effective infiltration (less losses to evaporation and runoff), especially important for the Korba region with a current rainfall capture quota thought to be less than 10% of annual rainfall; incorporation of water quality (salinity levels) of the irrigation water, and soil zone salinization effects resulting from this water.

In summary, this study has used numerical simulation to analyze some of the interactions and possible mechanisms for saltwater intrusion in the Korba coastal plain. The approach undertaken to setting up an information management and modeling system for the Korba site, containing extensive (though incomplete) geospatial and hydrogeological data from various sources, is currently being applied to two other coastal aquifers in semi-arid regions (Sardinia, Italy and Sahel, Morocco) that are highly sensitive to severe degradation by saltwater intrusion. GIS and numerical models can be extremely useful tools for water resources management, but require consistent data support, in particular continuous monitoring of relevant parameters and processes. In these and future studies, the need for closer interaction and coordination between monitoring and modeling must therefore be encouraged.

Acknowledgements

This work has been funded by the AVICENNE Programme of the European Commission (grant number AVI-CT93-2-073) and by the Programme for International Cooperation for Development of the Sardinia Regional Authorities (L.R. 19/96). The authors wish to thank Fabio Bettio for his generous assistance with the visualizations of the simulation results.

References

Bear, J., *Hydraulics of Groundwater.* McGraw-Hill, New York, NY, 1979.

Bear, J., A. H.-D. Cheng, S. Sorek, D. Ouazar and I. Herrera (eds.), *Seawater Intrusion in Coastal Aquifers — Concepts, Methods and Practices.* Kluwer Academic, Dordrecht, The Netherlands, 1999.

Brooks, R. H. and A. T. Corey, Hydraulic properties of porous media. Hydrology Paper 3, Colorado State University, Fort Collins, CO, 1964.

Collins, M. A. and L. W. Gelhar, Seawater intrusion in layered aquifers, *Water Resour. Res.* 7(4), 971–979, 1971.

Essaid, H. I., A multilayered sharp interface model of coupled freshwater and saltwater in coastal systems: Model development and application, *Water Resour. Res.* 26(7), 1431–1454, 1990.

Frind, E. O., Simulation of long-term transient density-dependent transport in groundwater, *Adv. Water Resour.* 5, 73–88, 1982.

Galeati, G., G. Gambolati and S. P. Neuman, Coupled and partially coupled Eulerian-Lagrangian model of freshwater-seawater mixing, *Water Resour. Res.* 28(1), 149–165, 1992.

Gambolati, G., M. Putti and C. Paniconi, Three-dimensional model of coupled density-dependent flow and miscible salt transport. In: Bear, J., A. H.-D. Cheng, S. Sorek,

D. Ouazar and I. Herrera (eds.) *Seawater Intrusion in Coastal Aquifers — Concepts, Methods and Practices* chapter 10, 315–362, Kluwer Academic, Dordrecht, The Netherlands, 1999.

Giacomelli, A., C. Paniconi, I. Khlaifi and J. Tarhouni, A modular approach to the Korba aquifer seawater intrusion study, 1, GIS field data analysis. In: De Breuck, W. and L. Walschot (eds.) *Proceedings of the 15th Salt-Water Intrusion Meeting.* Natuurwetenschappelijk Tijdschrift (Flemish Journal of Natural Science), Ghent, Belgium. Volume 79, pp 220–226, 1999.

Huyakorn, P. S., P. F. Andersen, J. W. Mercer and H. O. White, Saltwater intrusion in aquifers: Development and testing of a three-dimensional finite element model, *Water Resour. Res.* 23(2), 293–312, 1987.

Khlaifi, I., *Contribution à l'étude de l'intrusion marine par un modèle de transport tridimensionnel: Interfaçage avec des systèmes d'informations géographiques.* Master's thesis, Institut National Agronomique de Tunisie, Département de Génie Rural, Eaux et Forêts, 1998.

Kolditz, O., R. Ratke, H.-J. G. Diersch and W. Zielke, Coupled groundwater flow and transport: 1. Verification of variable density flow and transport models, *Adv. Water Resour.* 21(1), 27–46, 1998.

Lecca, G., I. Khlaifi, J. Tarhouni and C. Paniconi, Modeling seawater intrusion in the Korba aquifer (Tunisia). In: Burganos, V. N., G. P. Karatzas, A. C. Payatakes, C. A. Brebbia, W. G. Gray and G. F. Pinder (eds.) *Proceedings of the XII International Conference on Computational Methods in Water Resources, Vol. 2, Computational Methods in Surface and Ground Water Transport.* Computational Mechanics Publications, Southampton, UK, pp 209–216, 1998.

Mercer, J. W., S. P. Larson and C. R. Faust, Simulation of salt-water interface motion, *Ground Water* 18, 374–385, 1980.

Paniconi, C. (ed.), *Interim Report on the Preliminary Study of Soil and Aquifer Degradation from Seawater Intrusion in the Coastal Areas of Tunisia, Morocco, and Sardinia (RAS, L.R. 19/96).* Center for Advanced Studies, Research and Development in Sardinia (CRS4) and Ente Autonomo Flumendosa (EAF), Cagliari, Italy, 1999.

Paniconi, C. and M. Putti, A comparison of Picard and Newton iteration in the numerical solution of multidimensional variably saturated flow problems, *Water Resour. Res.* 30(12), 3357–3374, 1994.

Paniconi, C., S. Kleinfeldt, J. Deckmyn and A. Giacomelli, Integrating GIS and data visualization tools for distributed hydrologic modeling, *Transactions in GIS* 3(2), 97–118, 1999.

Putti, M., W. W.-G. Yeh and W. A. Mulder, A triangular finite volume approach with high-resolution upwind terms for the solution of groundwater transport equations, *Water Resour. Res.* 26(12), 2865–2880, 1990.

Putti, M. and C. Paniconi, Picard and Newton linearization for the coupled model of saltwater intrusion in aquifers, *Adv. Water Resour.* 18(3), 159–170, 1995.

Schmorak, S. and A. Mercado, Upconing of freshwater–seawater interface below pumping wells, Field study, *Water Resour. Res.* 5(6), 1290–1311, 1969.

Ségol, G., *Classic Groundwater Simulations: Proving and Improving Numerical Models.* PTR Prentice Hall, Englewood Cliffs, NJ, 1993.

Sherif, M. M. and V. P. Singh, Saltwater intrusion. In: Singh, V. P. (ed.) *Hydrology of Disasters* chapter 10, 269–316, Kluwer Academic, Dordrecht, Holland, 1996.

Strack, O. D. L., A single-potential solution for regional interface problems in coastal aquifers, *Water Resour. Res.* 12(6), 1165–1174, 1976.

van Genuchten, M. T. and D. R. Nielsen, On describing and predicting the hydraulic properties of unsaturated soils, *Ann. Geophys.* 3(5), 615–628, 1985.

Voss, C. I. and W. R. Souza, Variable density flow and solute transport simulation of regional aquifers containing a narrow freshwater-saltwater transition zone, *Water Resour. Res.* 23(10), 1851–1866, 1987.

Wirojanagud, P. and R. J. Charbeneau, Salt water upconing in unconfined aquifers, *J. Hydraulic Engrg., ASCE* 111, 417–434, 1985.

Zienkiewicz, O. C., *The Finite Element Method.* McGraw-Hill, New York, NY, 1986.

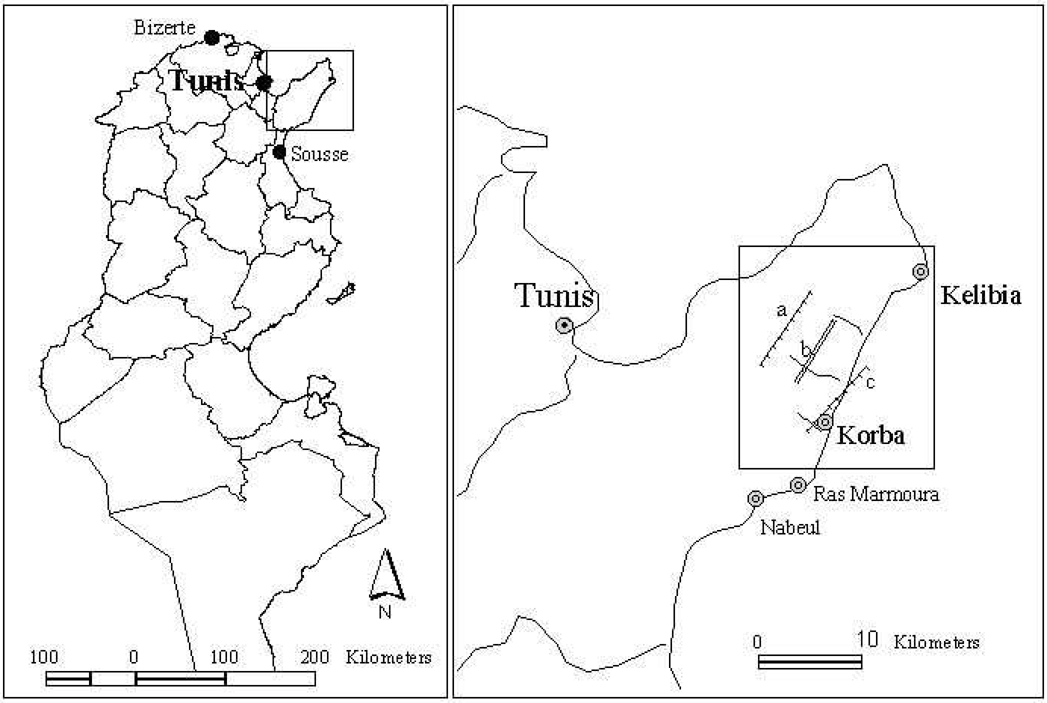

Figure 1: Location map of the Korba coastal plain in northeastern Tunisia on the Mediterranean Sea (left) and enlargement showing the population centers and the main hydrographic — ephemeral streams — and geological — anticline (a and c) and syncline (b) — features (right).

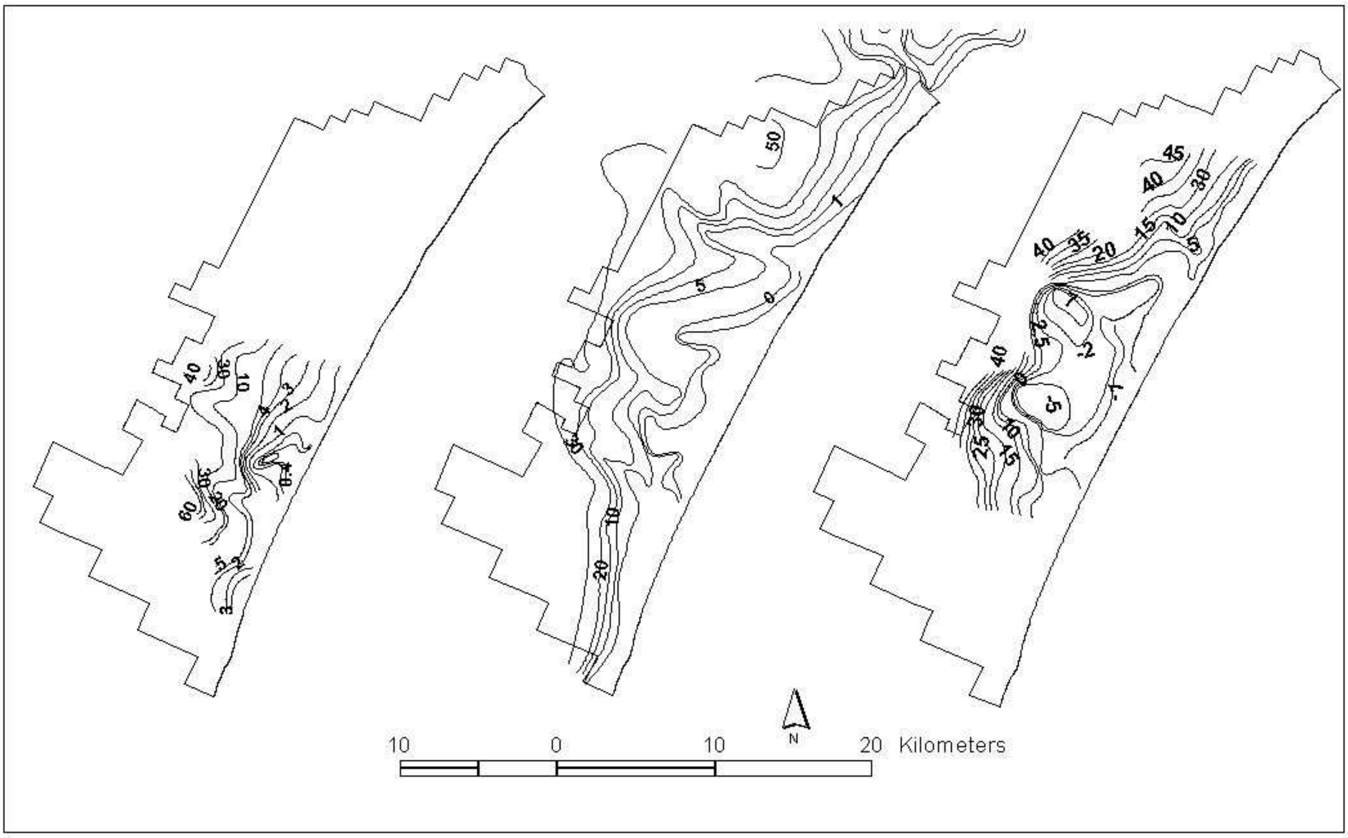

Figure 2: Observed water table levels (m a.s.l.) from 1962 (left), 1977 (middle), and 1996 (right) well data for the modeled area showing a general decline in piezometric levels over the 35-year period, and significant drawdown in zones of heavy groundwater pumping. With reference to Figure 1, the modeled area comprises the coastal region between Kelibia and (just north of) Ras Marmoura and is delimited in the west by the Djbel Sidi AbedErrahmen mountains (anticline "a").

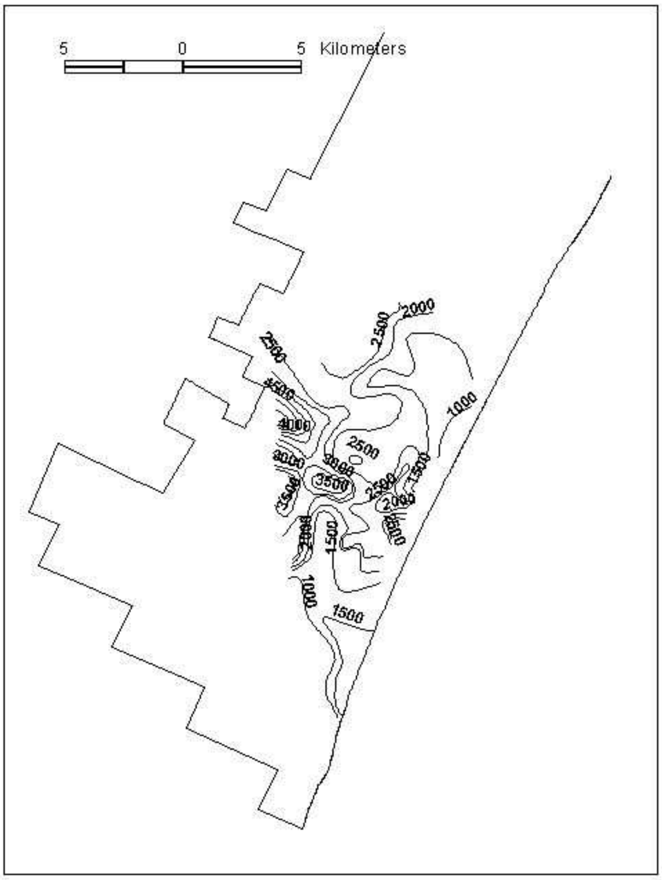

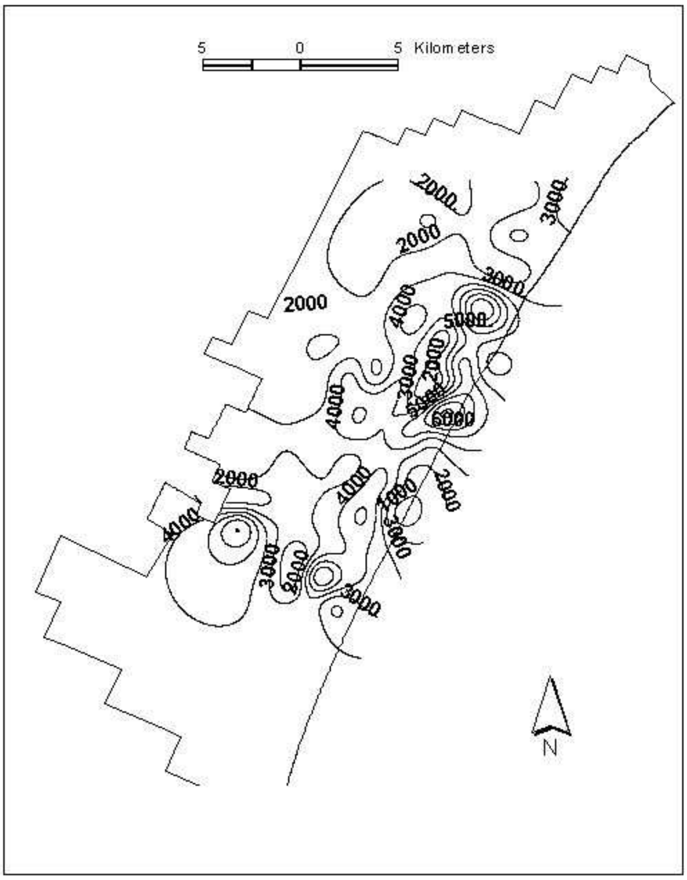

Figure 3: Observed salinity levels (mg/l) from 1962 (left) and 1996 (right) well data showing salinization trend especially near the coast and in zones of heavy groundwater pumping.

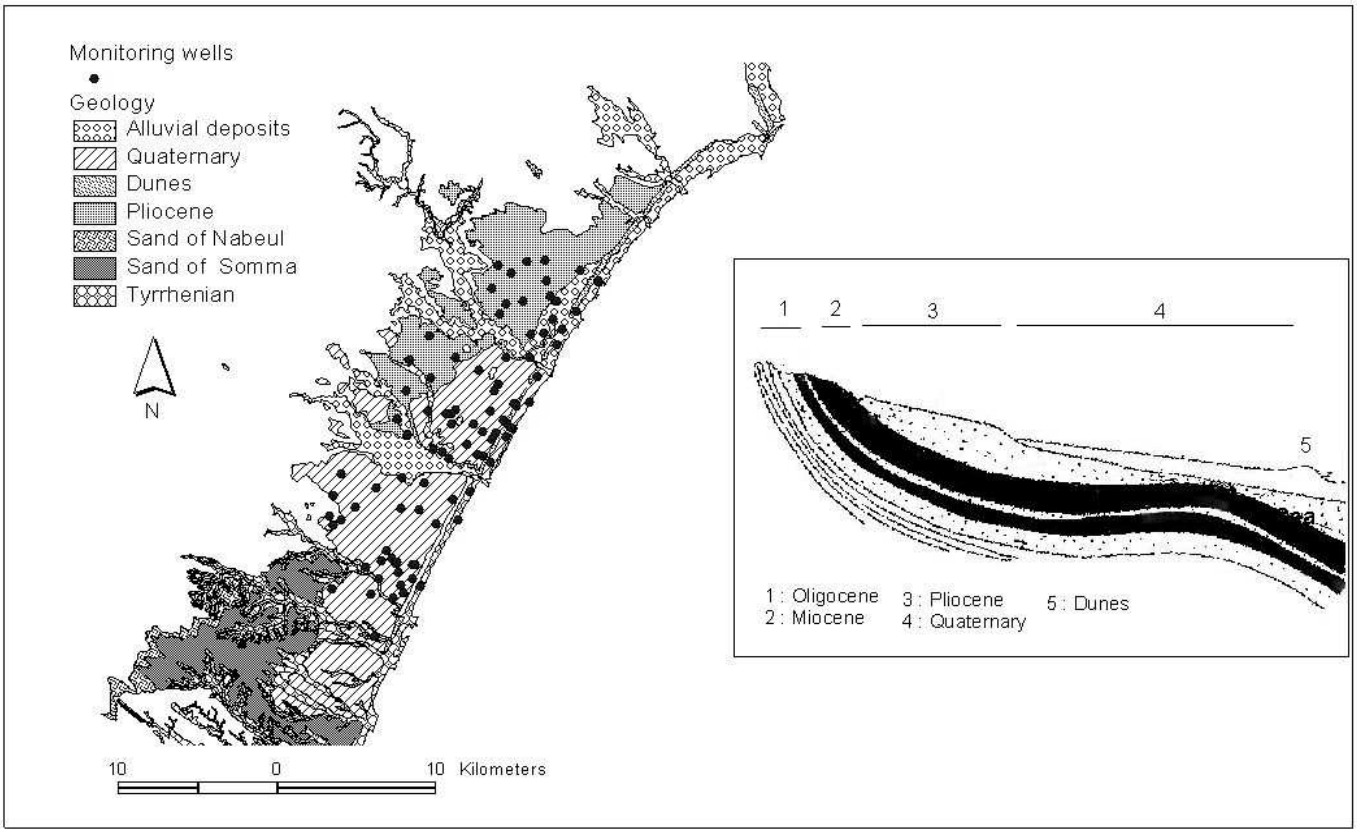

Figure 4: Simplified geological map of the Korba study area derived by aggregation of surface geological features into dominant units (left); vertical geological cross section perpendicular to the coast and passing roughly midway through the aquifer showing the anticline, syncline, and dune formations that determine the shape and varying thickness of the Quaternary–Pliocene unconfined aquifer, along with underlying formations (right).

Figure 5: Shaded relief map (left) of the modeled area showing the hilliest southwestern portion (max elevation 161 m a.s.l.) and the comparatively flat central region of the coastal plain. The right image shows aquifer thickness contours overlain on a detailed map of the channel network. The aquifer thickness is highly variable, with minimum depth 24 m, maximum 151 m, and mean 83.5 m.

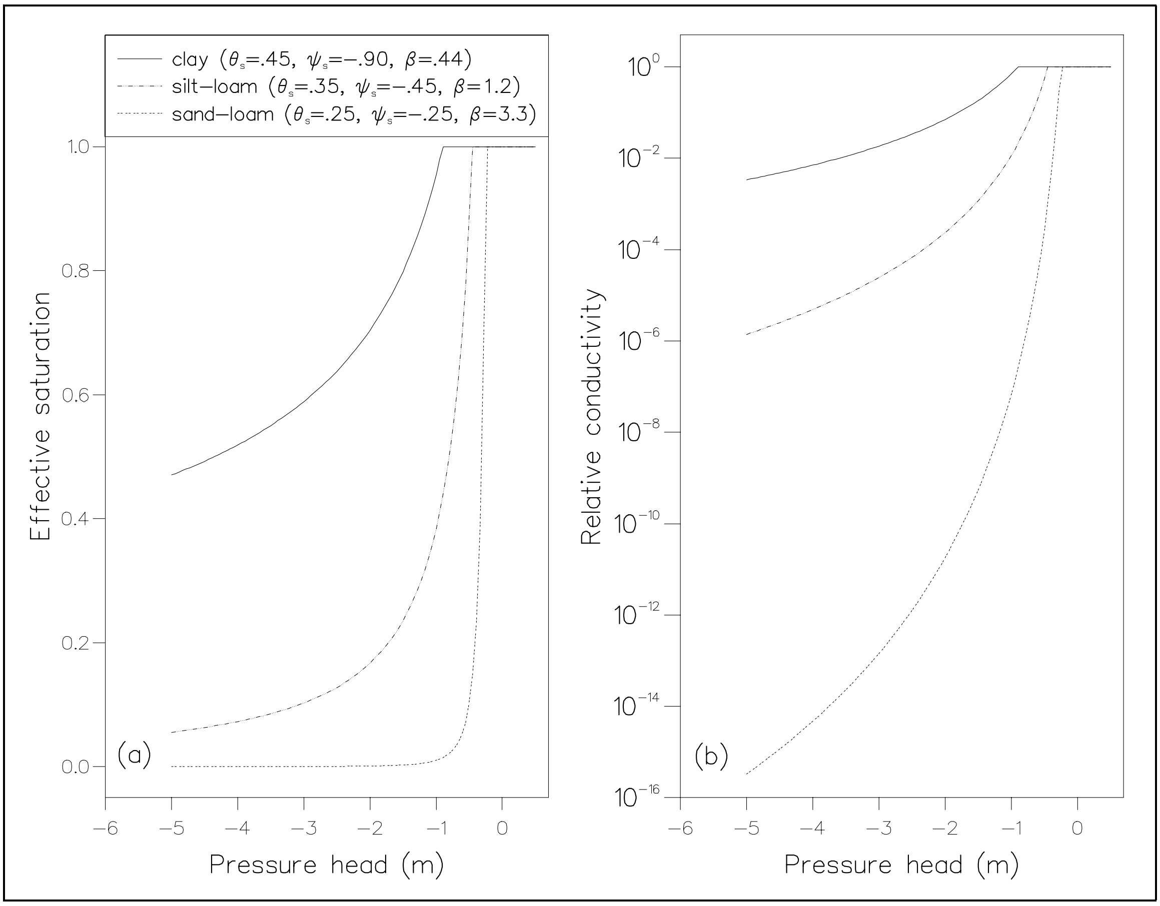

Figure 6: Unsaturated zone characteristic relationships between pressure head and effective saturation (a) and between pressure head and relative hydraulic conductivity (b), along with Brooks-Corey parameters, for three representative soil types: clay, silt-loam, and sand-loam.

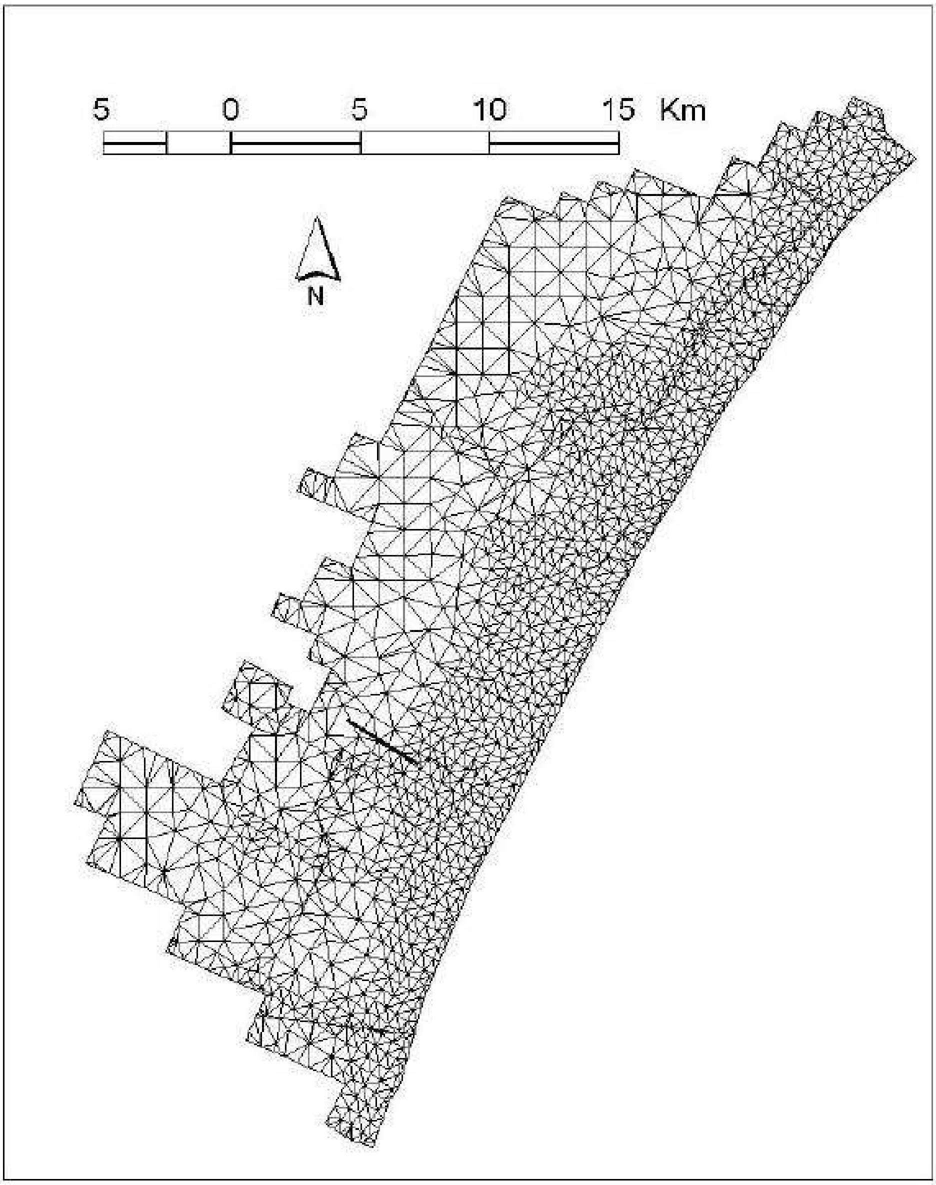

Figure 7: Surface discretization of the modeled area into 2917 triangles, with the smallest elements near the coast and around important pumping well clusters. This nonuniform surface grid was replicated vertically for 6 layers of varying thickness (thinnest layers near the surface) to yield a three-dimensional mesh containing 52506 tetrahedral elements and 11501 nodes.

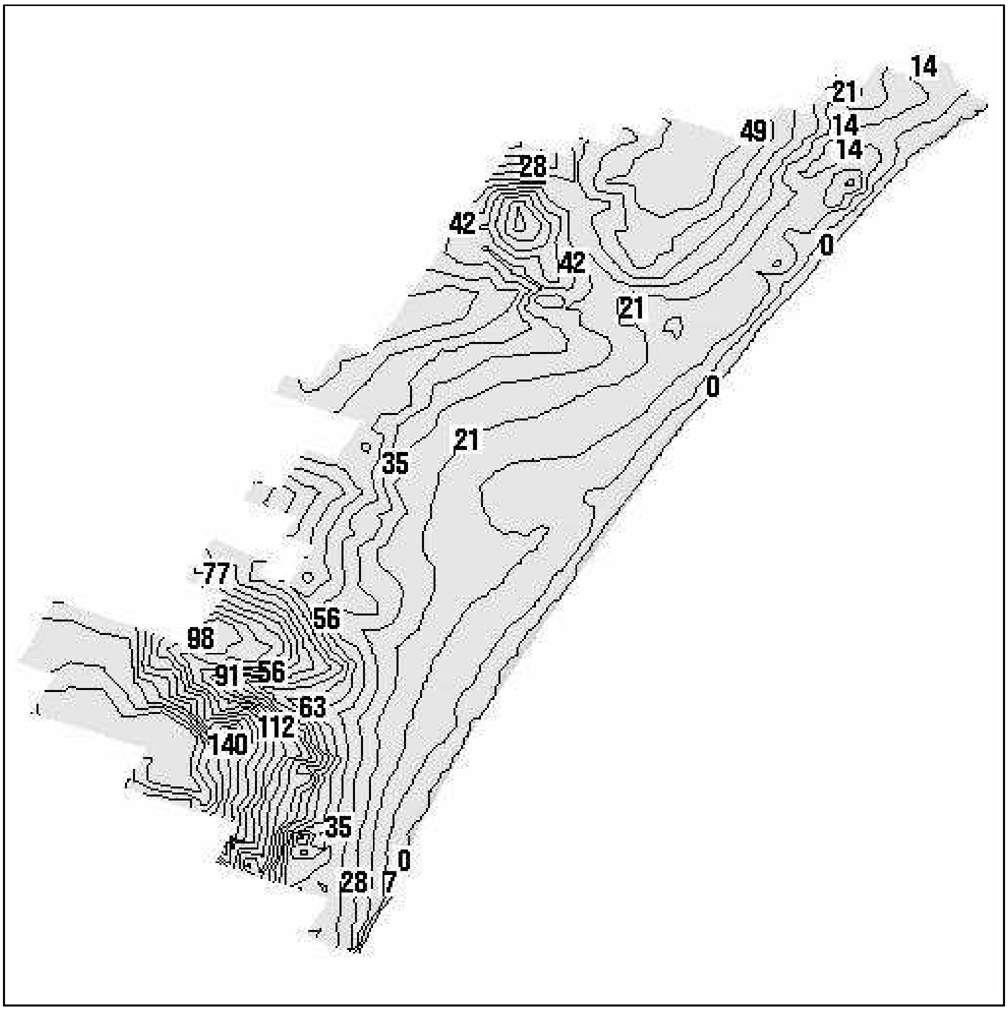

Figure 8: Water table levels (m a.s.l.) from the steady state flow simulation used to calibrate the model to 1962 "initial conditions" for subsequent 35-year transient flow and transport simulations.

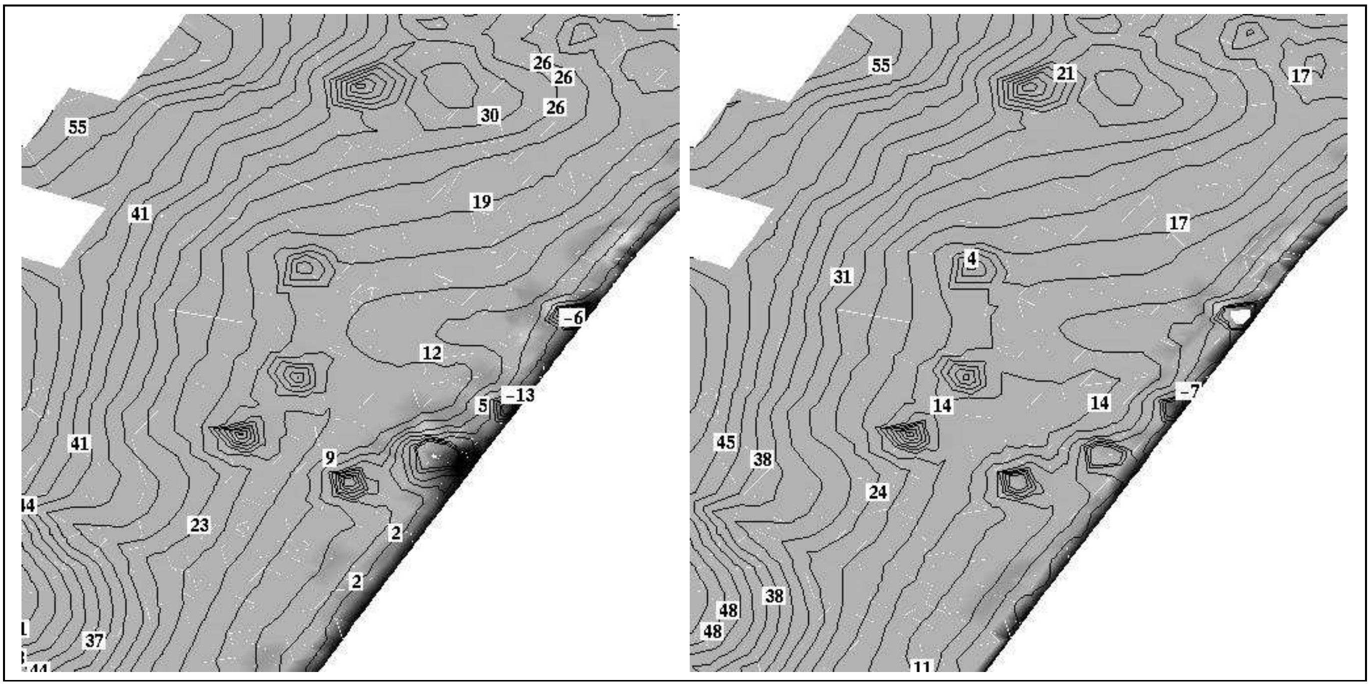

Figure 9: Water table levels (contour lines in m a.s.l.) and zones of high salinity along the coast (in black) for two cases of a 35-year transient coupled simulation with pumping from 10 wells. In the left plot the overall groundwater pumping rate is increased linearly over the entire simulation period, from 0 to 7.2×10^{6} m^3/yr; in the right plot this same pumping regime is applied, and in addition a uniform artificial recharge rate of 3×10^{6} m^3/yr is introduced after 25 years at one well near the coast, producing a retreating saltwater front and a reduced drawdown.

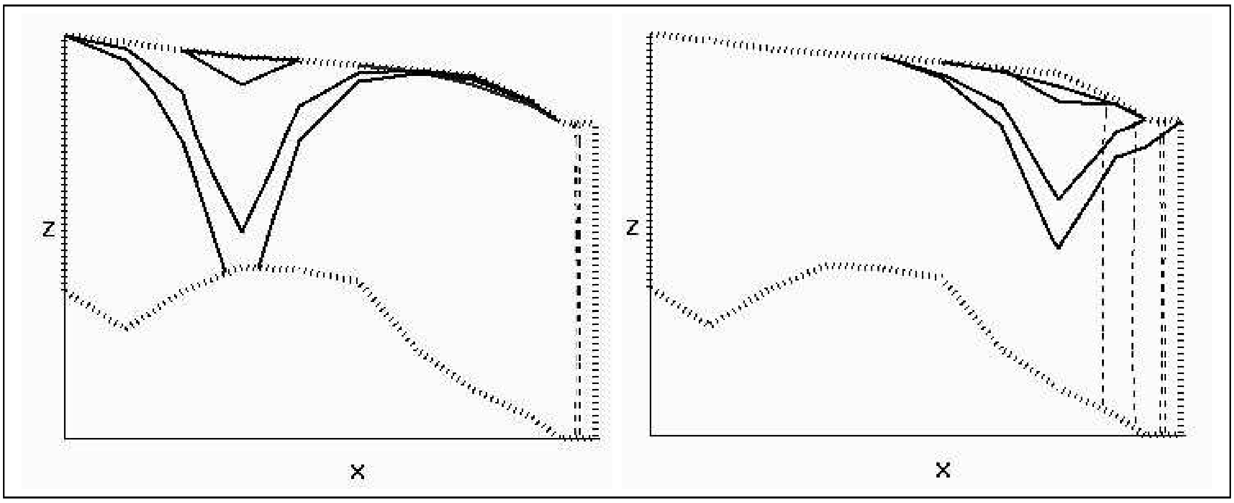

Figure 10: Simulation results for two experiments plotted as vertical cross sections perpendicular to the coast and passing through the town of Korba, comparing the groundwater drawdown (solid lines) and saltwater front migration (dashed lines) from inland (left) and coastal (right) pumping regimes and illustrating the interaction between the unsaturated zone and the saltwater–freshwater interface. The two plots show water table levels and 0.5 normalized salinity isolines at times 1, 6, 25, and 35 years in response to pumping from a single well at a rate that increases linearly over the 35-year simulation period from 0 to 0.91×10^6 m^3/yr. In this and the following figures the depth of the aquifer at the coast (z-axis) is approximately 100 m while the length (x-axis) is about 5 km.

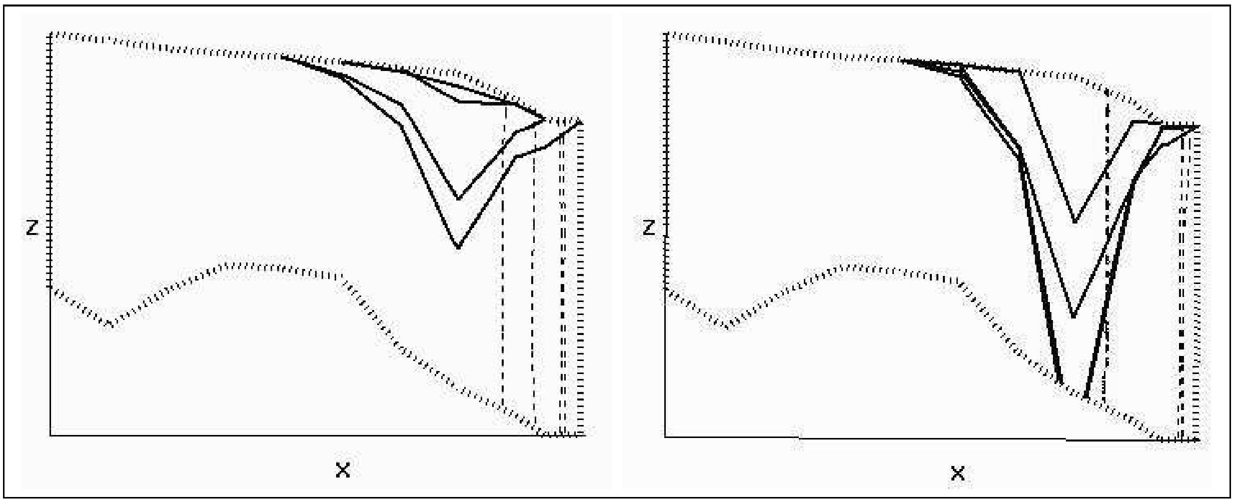

Figure 11: Simulation results for two experiments plotted as vertical cross sections perpendicular to the coast and passing through the town of Korba, comparing the groundwater drawdown (solid lines) and saltwater front migration (dashed lines) from soils with differing textures and infiltration capacities: a sand-loam soil/aquifer with effective infiltration of 22 mm/yr (left) and a clay soil/aquifer with effective infiltration of 15 mm/yr (right). The two plots show water table levels and 0.5 normalized salinity isolines at times 1, 6, 25, and 35 years in response to pumping from a single well at a rate that increases linearly over the 35-year simulation period from 0 to 0.91×10^6 m^3/yr.

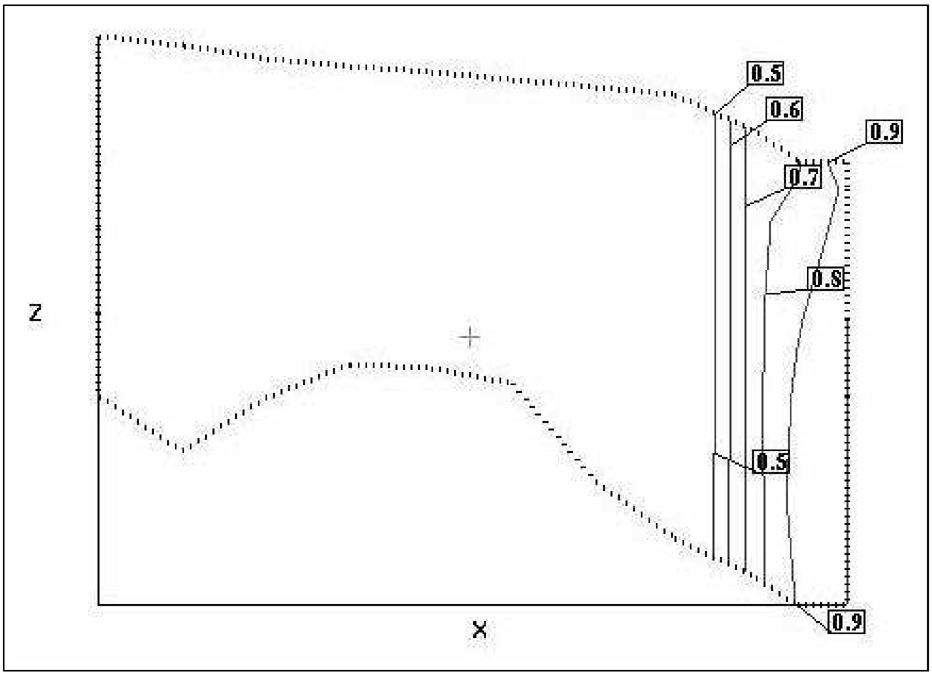

Figure 12: Concentration isolines at time 35 years on the vertical cross section for the simulation of coastal pumping from a single well in a clay soil/aquifer, showing the shape and width of the disperse saltwater–freshwater interface.